High Resolution Electron Microscopy Characterization of Nitrides of Iron and Iron Alloys

G. Hinojosa, P.S. Schabes-Retchkiman, and J. Oseguera

(Submitted 6 November 1997; in revised form 13 February 1998)

A study of nitride-phase formation in alloys nitrided by glow discharge plasma nitriding was performed by high-resolution electron microscopy. The iron and steel samples were nitrided above and below the eutectoid transformation point (590 °C). After nitriding, the samples were annealed for several treatment times at 400 °C. The microstructure and identification of the iron nitrided phases formed by nitriding and annealing were investigated by x-ray diffraction (XRD), optical microscopy (OM) and mainly high resolution electron microscopy (HREM) in a JEOL-4000EX high resolution microscope at 400 kV. The results of the characterization show a surface ε compact nitride layer, which is transformed into ε + γ during cooling. The tempering process affects the surface hardness of the samples. After an initial increase relative to the untreated sample, the microhardness diminishes after long treatment times. This behavior is correlated with the α″ phase appearance, growth, and transformation.

Keywords HREM, iron nitrides, plasma nitriding

1. Introduction

Formation of compact nitride layers on the surface of steel pieces significantly enhances the tribological properties of the pieces and improves their resistance to corrosion (Ref 1). Nitrogen desaturation in the ferritic matrix during cooling leads to the formation of iron nitrides. Precipitation of nitrides in the ferritic matrix contributes to the enhancement of the mechanical properties; distribution of precipitates in the ferritic matrix actively blocks the dislocation movement.

Thermal treatments applied after the nitrogen solubilization in the ferrite produces precipitates. The type of precipitates that are obtained after plasma nitriding and thermal treatments was characterized, and the microstructural changes associated with the nitrides during tempering in pure iron and in a carbon steel (AISI 1010) are presented using optical microscopy (OM), transmission electron microscopy (TEM), and high resolution electron microscopy (HREM).

2. Experimental Methods

Nitriding of the iron and steel samples was performed in the experimental chamber described in Ref 2. The weakly ionized plasma is created by means of a diode electrical discharge of double alternating field. The current density varied from 5 to 30 A/m^2. The treatment temperature for iron was 670 °C, close to, but above, the eutectoid transformation temperature and for steel close to 570 °C (below the eutectoid temperature). The samples were nitrided for 3 h for iron and 4 h for the 1010 steel at 400 Pa operational pressure with 22/10 N_2/H_2 mixtures.

The iron and steel samples were cylindrical in shape, 1 cm in diam, and 1 cm in height. Chemical analysis of the samples yielded the following compositions: ARMCO iron, <800 ppm Mn, <200 ppm C, <200 ppm P, and <150 ppm S; SAE-AISI 1010 steel with 0.11 wt% C, 0.36 wt% Mn, 0.02 wt% P, and 0.016 wt% S. The annealing treatments were done at 400 °C from 0 to 128 h for iron and from 0 to 16 h for steel.

Cross-sectional transmission electronmicroscopy (XTEM) samples were prepared by mechanical polishing of the specimens, followed by ion milling. The final ion-milling step was performed at grazing incidence to avoid preferential sputtering of one nitride species over the others. Some samples were prepared by grinding with the tripod method to transparency. The microstructure and phase composition of the formed layers were investigated using x-ray diffraction (XRD), conventional TEM in a JEOL 1210 TEM, and HREM in a JEOL-4000EX high resolution electron microscope at 400 kV.

3. Results and Discussion

3.1 Iron Samples

Figure 1 shows optical micrographs of the cross sections of iron pieces. Figure 1(a) shows the precipitation of α″ $Fe_{16}N_2$, preferentially near to the ferritic grain boundary in the ferritic matrix. The nitrides are obtained after cooling of the sample inside the reactor. The partial transformation of the austenite layer during the cooling process is also shown. Figure 1(b) corresponds to a sample annealed for 32 h. In contrast with Fig. 1(a) the formation of γ′-Fe_4N_{1-x} needles is apparent. The austenite layer transformation is also shown.

During the aging treatment, the vast majority of the α″-$Fe_{16}N_2$ nitrides are transformed to the α + γ′ microstructure in the ferritic matrix. The HREM image of an α″-$Fe_{16}N_2$ particle in the aged sample is shown in Fig. 2(a). In Fig. 2(b), a magni-

G. Hinojosa, ITESM-CEM, DGI, Apdo. Postal 18, Atizapan, Mexico, 52926, Mexico; **P.S. Schabes-Retchkiman,** Instituto de Fisica, U.N.A.M., Apdo. Postal 20-364, Mexico, D.F. 01000, Mexico; and **J. Oseguera,** I.N.I.N., Centro Nuclear "Nabor Carrillo," Km. 36.5 Carr. Fed. México-Toluca, 52045, Salazar, Edo. De México, Mexico.

fied and processed image of the zone within the white square in Fig. 2(a) is shown. The white dots correspond to the iron periodicity in the 2 by 2 by 2 cell of the ferritic matrix. Figure 2(c) shows a multilayer simulation of a <001> oriented, 10 nm thick α'' particle formed by considering the $Fe_{16}N_2$ cell. This cell has a fully ordered nitrogen atom arrangement in a slightly distorted body-centered cubic atom array with $a = 0.572$ nm and $c = 0.629$ nm (Ref 3, 4). The simulation shows that the white dots correspond to iron atom positions in the body-centered tetragonal α'' structures. The distance between dots corresponds to d (100) in α''. This arrangement of iron atoms comprises 2 by 2 by 2 unit cells of the ferrite lattice. The small α'' precipitate shows several types of defects: dislocations and planar defects, that is, antiphase boundaries or twins within it. The particle is observed to be coherent with the matrix. Concomitant with the α'' transformation, a change of hardness in the diffusion zone is observed as a function of the annealing time (Ref 3, 5).

In Fig. 3(a), a HREM image corresponding to the topmost layers of the iron sample is shown. In this image, the $\varepsilon \leftrightarrow \gamma'$ transformation can be observed in the nitride (Ref. 6, 7). Figure 3(b) corresponds to a magnification of the transformation zone of 3(a). The image simulation shown in Fig. 3(c) shows that the white fringes correspond to iron in the hexagonal close-packed cell of the ε nitride.

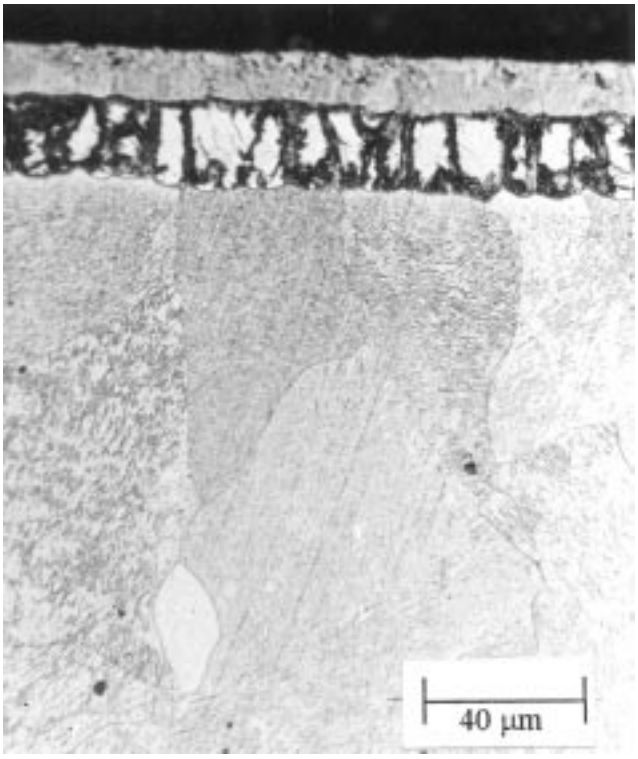

(a)

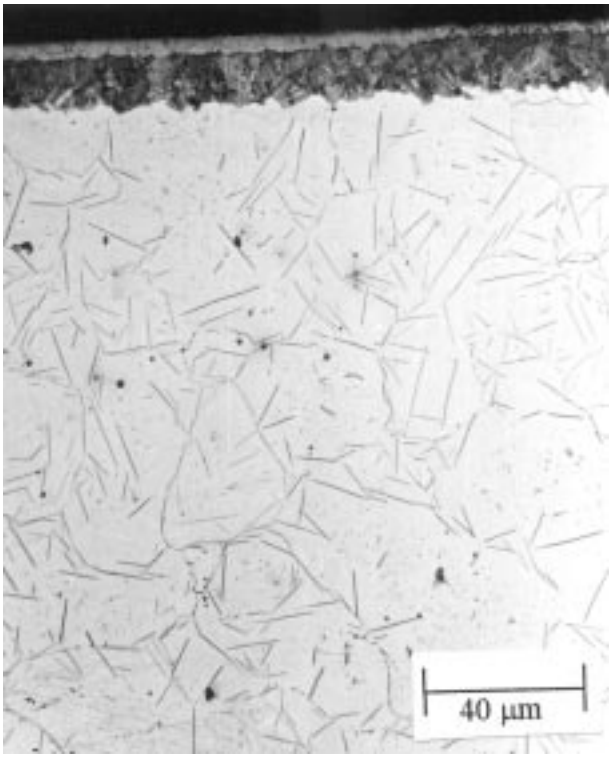

(b)

Fig. 1 Optical micrographs of cross sections of nitrided iron. (a) Sample after cooling, showing compact layers at the top, diffusion zone, and α'' precipitation. (b) Sample after annealing of several hours. γ' precipitation is shown as long needles.

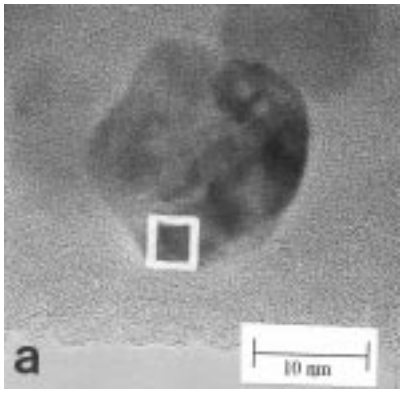

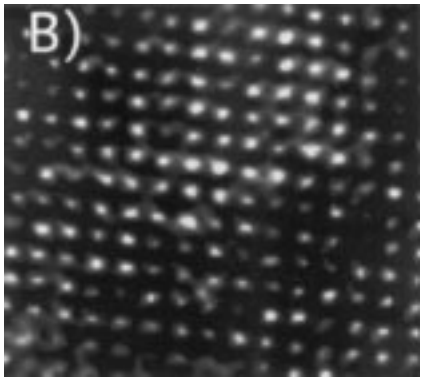

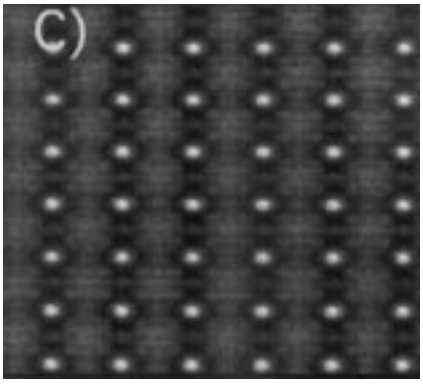

Fig. 2 (a) HREM image of a α'' precipitate. (b) Magnified and processed image of the marked area in (a). (c) Calculated image for a 10 nm thick, –50 nm defocus, 400 keV image of <001> oriented α'' $Fe_{16}N_2$ particle. The calculated and experimental images match closely.

3.2 Steel Samples

Figure 4 shows the image of a cross section of the 1010 steel aged at a temperature of 400 °C for 0.5 h. In the surface of the sample a ε-$Fe_{2-3}N$ nitride layer is shown. In the nitrogen diffusion zone in the ferrite, needle precipitation of nitrides is shown.

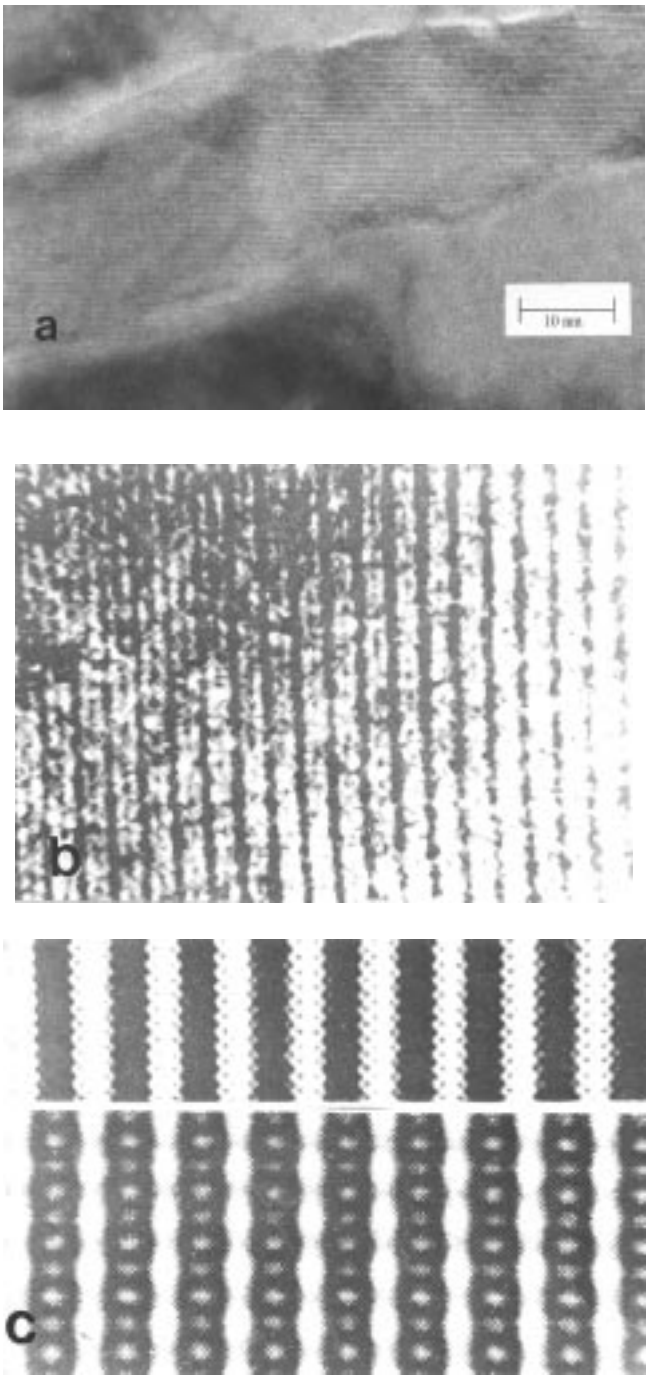

Fig. 3 (a) HREM image of topmost layers in iron, showing a platelet. (b) Magnified and processed image showing the ε to γ′ transformation zone. (c) Simulated images of ε in <2110> orientation and γ′ in <011> orientation. Note the excellent match with the experimental image.

In the iron, during the aging treatment, the majority of α″ are transformed in the ferritic matrix. Figure 5(a) shows a HREM image of a α″-$Fe_{16}(N,C)_2$ precipitate. The size of this precipitate is similar to that shown in Fig. 2(a), that is, approximately 20 nm. Figure 5(b) corresponds to an enlargement of the previous image. The associated optical diffractogram corresponds to that of α″ nitride. Remarkably, the particle shown exhibits (as in iron) twin boundaries, reminiscent of those observed by HREM in evaporated gold icosahedral multiply-twinned particles (Ref 8, 9). These particles form with a disclination down the center. It is possible that in iron or steel, their growth is such to accommodate stress within the matrix. Also noted, the precipitate is coherent with the matrix.

The α″-$Fe_{16}(C,N)_2$ precipitates grow with the annealing treatment from an average of 15 to 45 nm for 0.5 h treatment times before decomposing for longer treatment times.

In Fig. 6(a), a HREM image of the topmost layers in annealed 1010 steel is shown. In contrast with Fig. 3(a), corresponding to iron, the γ′↔ε in the same precipitate was not observed. Figure 6(b) is an enlargement of Fig. 6(a). The obtained diffractogram corresponds to γ′ nitride in the <111> orientation.

Nitride formation in the ferritic zone is determined by the stable or metastable thermodynamical equilibrium as represented in the phase diagrams. For iron nitriding, nitride formation is determined by the Fe-N system phase diagram. For steel nitriding, ternary Fe-C-N determines the type of nitrides that are formed.

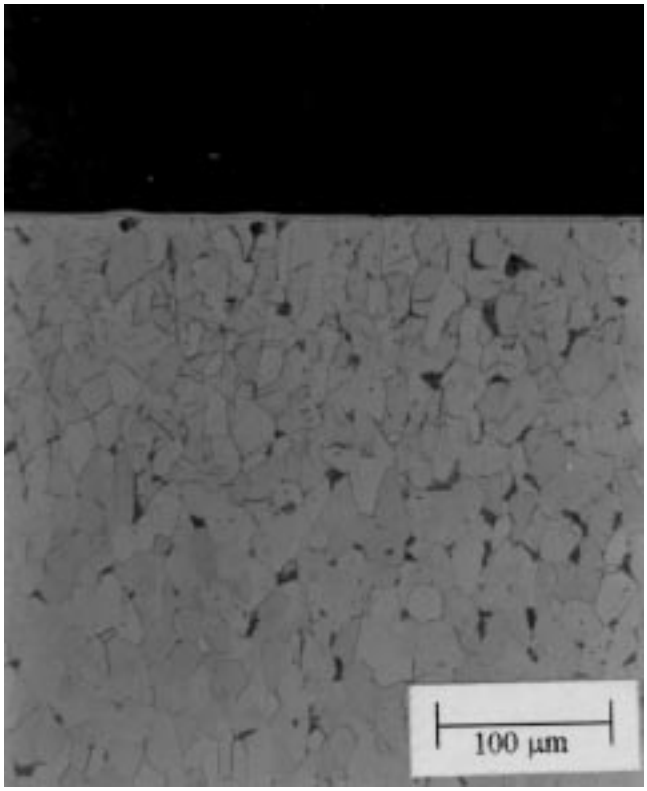

Fig. 4 Optical micrograph of a cross section of nitrided 1010 steel sample after annealing for 0.5 h. Needle precipitation is shown.

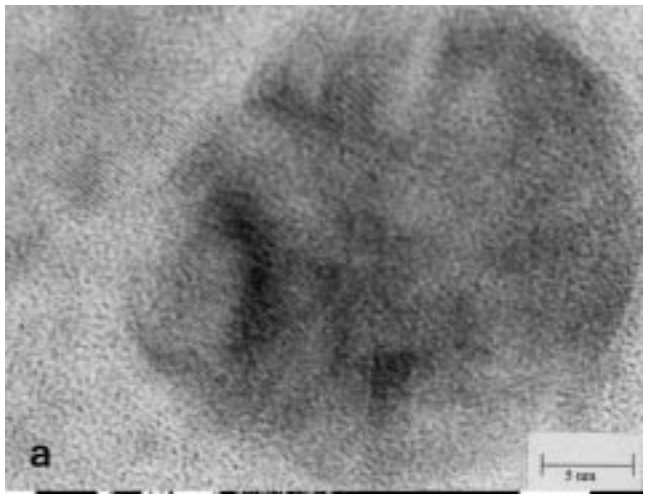

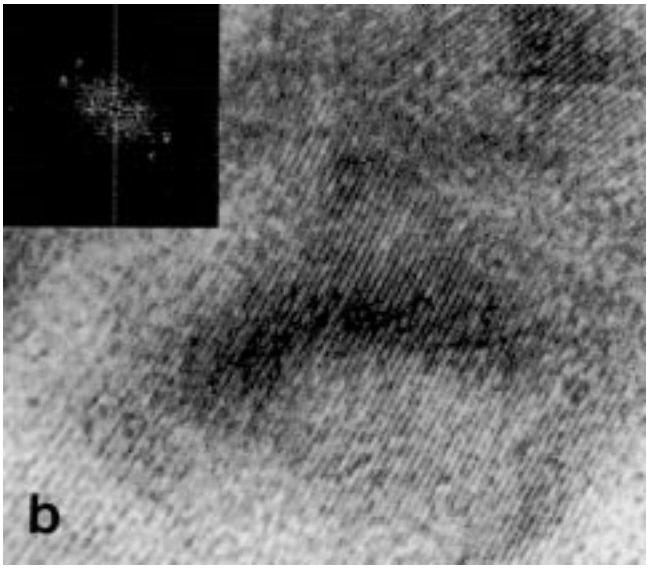

Fig. 5 (a) HREM image of α″ precipitate. (b) Enlargement of twin boundary in (a), inset diffractogram.

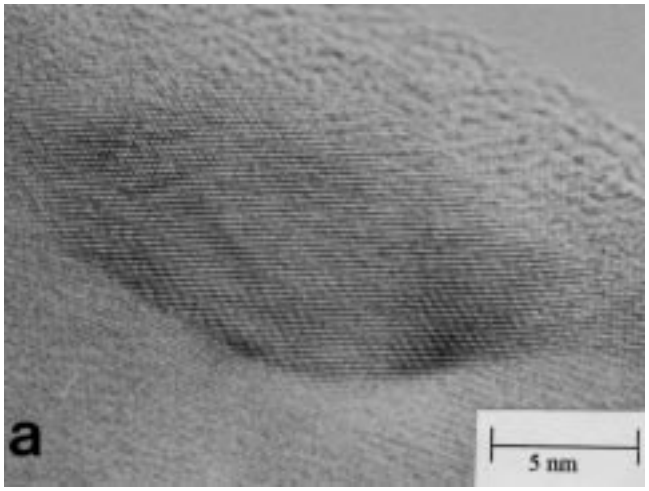

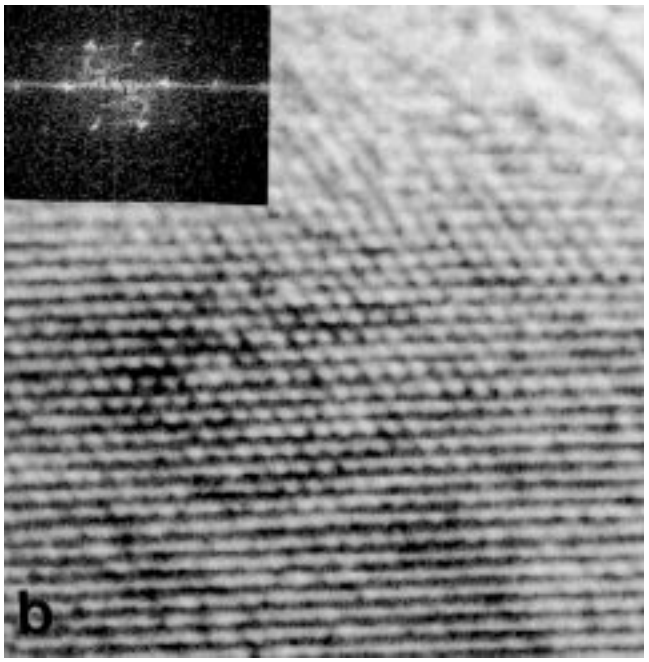

Fig. 6 (a) HREM of γ′ precipitate after 4 h of annealing time. (b) Enlargement of top left corner of the precipitate, inset, diffractogram

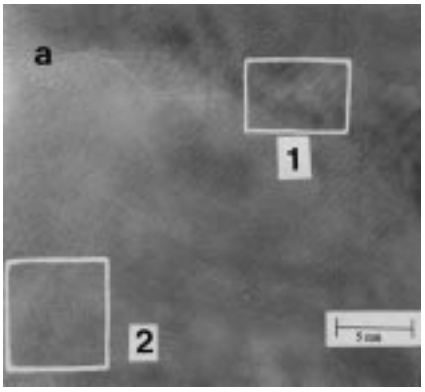

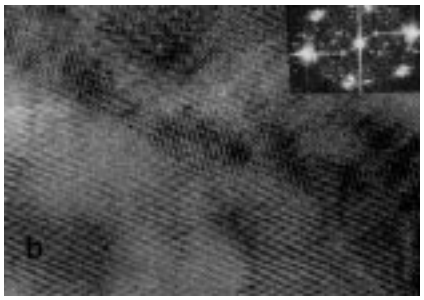

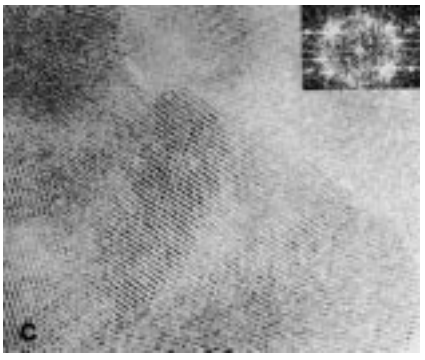

Fig. 7 (a) HREM image of the topmost layers in cooled sample. (b) Magnified processed image of region marked 1 in (a) matches with the ε phase. (c) Magnified processed image of region marked 2 in (a) corresponds to a γ′ defective precipitate.

Finally in Fig. 7(a), regions of coexistence of γ' and ε in the ferritic matrix of 1010 steel are shown. Figure 7(b) shows an ε phase zone; the precipitates are clearly identified as ε in the <0001> orientation. Figure 7(c) shows a highly defected γ' precipitate in the zone marked as 2 in Fig. 7(b). The shape and size of the precipitates depend strongly on the chemical equilibrium in the interfaces and of the structure of each phase.

Acknowledgments

We are grateful to CONACyT for financial support received under grant 3334-a. Technical support by L. Rendón and Angel Flores is also appreciated.

References

1. J. Grosch, J. Morral, and M. Schneider, *Carburizing and Nitriding with Atmospheres,* ASM International, 1995
2. J. Oseguera, A. Bravo, and V. Romero, *Proc. IBEROMET II,* Vol 1, 1992, p 857
3. G. Hinojosa, J. Oseguera, O. Salas, and P.S. Schabes-Retchkiman, Microscopical Characterization of α'' $Fe_{16}N_2$ Obtained by Plasma Assisted Processes, *Scr. Mater.,* Vol 34 (No. 1), 1996, p 141-145
4. K.H. Jack., *Proc. R. Soc.,* Vol A 208, 1951, p 206
6. M. Palacios et al., *Surf. Coat. Technol.,* Vol 76, 1995, p 377
5. D. Gerardin, H. Michel, and M. Gantois, *Scr. Metall.,* Vol 11, 1977, p 557
7. M. El Hajjaji, H. Michel, and M. Gantois, *Scr. Metall.,* Vol 17, 1983, p 879
8. P.S. Schabes-Retchkiman, A. Gomez, G. Vazquez-Polo, and M. Jose-Yacaman, Microdiffraction and Lattice Resolution Studies of Five Fold Symmetry Gold Particles, *J. Vac. Sci. Technol.,* Vol A2 (No. 1), 1984, p 22
9. M. Jose-Yacaman, R. Herrera, A. Gomez, S. Tehuacanero, and P.S. Schabes-Retchkiman, Decagonal and Hexagonal Structures in Small Gold Particles, *Surf. Sci.,* Vol 237, 1990, p 248